Received: 12 February 2021 | Revised: 4 August 2021 | Accepted: 16 August 2021

DOI: 10.1111/gcb.15863

Global Change Biology WILEY

PRIMARY RESEARCH ARTICLE

Stimulation of N_2O emission via bacterial denitrification driven by acidification in estuarine sediments

Xiaoxuan Su[1] | Teng Wen[2] | Yingmu Wang[3] | Junshi Xu[4] | Li Cui[1] | Jinbo Zhang[2,5] | Ximei Xue[1] | Kai Ding[1] | Yijia Tang[6,7] | Yong-guan Zhu[1,8,9]

[1]Key Laboratory of Urban Environment and Health, Institute of Urban Environment, Chinese Academy of Sciences, Xiamen, China

[2]School of Geography, Nanjing Normal University, Nanjing, China

[3]College of Civil Engineering, Fuzhou University, Fuzhou, China

[4]Civil and Mineral Engineering, University of Toronto, Toronto, Ontario, Canada

[5]Key Laboratory of Virtual Geographic Environment, Ministry of Education, Nanjing Normal University, Nanjing, China

[6]School of Life and Environmental Sciences, The University of Sydney, Sydney, New South Wales, Australia

[7]Sydney Institute of Agriculture, Sydney, New South Wales, Australia

[8]University of the Chinese Academy of Sciences, Beijing, China

[9]State Key Laboratory of Urban and Regional Ecology, Research Center for Eco-Environmental Sciences, Chinese Academy of Sciences, Beijing, China

Correspondence
Yong-guan Zhu, 1799 Jimei Road, Xiamen 361021, China.
Email: ygzhu@iue.ac.cn

Funding information
Natural Science Foundation of China, Grant/Award Number: 42021005 and 42003060; Strategic Priority Research Program of Chinese Academy of Sciences, Grant/Award Number: Y9IXD21A10; China Postdoctoral Science Foundation, Grant/Award Number: 2019M662253

Abstract

Ocean acidification in nitrogen-enriched estuaries has raised global concerns. For decades, biotic and abiotic denitrification in estuarine sediments has been regarded as the major ways to remove reactive nitrogen, but they occur at the expense of releasing greenhouse gas nitrous oxide (N_2O). However, how these pathways respond to acidification remains poorly understood. Here we performed a N_2O isotopocules analysis coupled with respiration inhibition and molecular approaches to investigate the impacts of acidification on bacterial, fungal, and chemo-denitrification, as well as N_2O emission, in estuarine sediments through a series of anoxic incubations. Results showed that acidification stimulated N_2O release from sediments, which was mainly mediated by the activity of bacterial denitrifiers, whereas in neutral environments, N_2O production was dominated by fungi. We also found that the contribution of chemo-denitrification to N_2O production cannot be ignored, but was not significantly affected by acidification. The mechanistic investigation further demonstrated that acidification changed the keystone taxa of sedimentary denitrifiers from N_2O-reducing to N_2O-producing ones and reduced microbial electron-transfer efficiency during denitrification. These findings provide novel insights into how acidification stimulates N_2O emission and modulates its pathways in estuarine sediments, and how it may contribute to the acceleration of global climate change in the Anthropocene.

KEYWORDS
acidification, bacterial denitrification, fungal denitrification, microbial community, N_2O emission, nitrogen isotopes

1 | INTRODUCTION

Ocean acidification can disrupt the balance and functioning of marine ecosystems (Wannicke et al., 2018). It has been reported that acidification can decrease calcification rates of marine oysters (Waldbusser et al., 2011), weaken the homing ability of fish (Kroeker et al., 2013), and increase growth rates of macro-algae (Koch et al., 2013). In estuarine regions, acidification is becoming even more serious, owing to the weak capacity of buffering acidification and thus raises a global concern in recent decades (Feely et al., 2008; Hurd et al., 2018).

Estuarine ecosystems are experiencing high anthropogenic loadings of reactive nitrogen (N), resulting in not only

eutrophication (Pettay et al., 2020) but also profound impacts on N biogeochemical cycles, especially those related to climate change. In anoxic estuarine sediments, denitrification is known as an effective pathway for the removal of reactive N, but is accompanied by emitting a potent greenhouse gas, nitrous oxide (N_2O; Jung et al., 2019; Su et al., 2019a; Tan et al., 2020). It has been estimated that global oceans contribute 20%–30% of N_2O emissions (Sun et al., 2020; Tian et al., 2020). As denitrifier activities are sensitive to pH fluctuations (Rittmann & McCarty, 2001), acidification could disturb denitrification performance and greatly affect N_2O fluxes. For example, Rees et al. (2016) documented that N_2O production was closely linked to pH levels in cold seawater, but the potential mechanism was less explored. Recognizing the roles of acidification in N transformations and their associated N_2O emissions in estuarine sediments is thus important for controlling eutrophication and mitigating greenhouse gas across globally relevant scales. Despite the importance, the impacts of acidification on denitrification and its associated N_2O dynamics in estuarine ecosystems have rarely been investigated.

It is traditionally thought that bacterial denitrification is the major pathway for the removal of nitrate and the release of N_2O from sediments (Gao et al., 2020; Wang, Pi, Jiang, et al., 2020). However, recent studies have demonstrated that fungal denitrification may also contribute to N transformation and N_2O production (Seo & DeLaune, 2010; Wankel et al., 2017). In fact, unlike terrestrial ecosystems, the diversity and ecological function of fungal denitrifiers in aquatic ecosystems remain largely unexplored, particularly in estuarine ecosystems (Grossart et al., 2019). As fungal denitrifiers lack N_2O reductase (Mothapo et al., 2015), fungal denitrification may represent a more potent source of N_2O emission compared with bacterial denitrification. However, N_2O emissions from fungal sources have rarely been investigated in estuarine sediments, and fungal denitrification in response to acidification is also unexplored. This, therefore, limits the comprehensive evaluation of N_2O emission in estuarine ecosystems under global estuarine acidification. In addition, some evidence from laboratory experiments has suggested that abiotic pathways (chemo-denitrification, such as iron coupled with nitrate/nitrite) can also produce N_2O as a by-product (Jones et al., 2015; McTigue et al., 2016; Wei et al., 2019). Unfortunately, both fungal denitrification and chemo-denitrification have been frequently overlooked in complex ecosystems when estimating N_2O fluxes. Whether the chemo-denitrification in estuarine ecosystems could contribute to a greater emission of N_2O is largely unknown. We hypothesize that both the activity of fungal denitrifiers and the cycling of iron would be promoted in organic/N-rich and anoxic estuarine sediments and probably contribute to greater emissions of N_2O relative to bacterial sources (Wankel et al., 2017). Moreover, because of the different adaptabilities of bacterial and fungal denitrifiers under acidified and neutral environments (Rousk et al., 2010), the shift away from optimal pH conditions caused by acidification may affect bacterial, fungal, and chemo-denitrification differently and lead to a heterogeneity in N_2O emission patterns in estuarine sediments. Therefore, understanding the responses of biotic and abiotic denitrification to acidification is essential to evaluate N_2O emission in estuarine ecosystems under global ocean acidification.

Currently, it remains a challenge to predict N_2O production in complex estuarine ecosystems, owing to the difficulty in distinguishing various N_2O production pathways (Wankel et al., 2017). This study applied a N_2O isotopocules analysis together with respiration inhibition approaches to provide a broader perspective on N_2O cycling during denitrification in anoxic estuarine sediments (Maeda et al., 2017). A N_2O isotopocules technique is a promising tool to distinguish various N_2O production sources in natural ecosystems (Wankel et al., 2017; Zou et al., 2014). This is because N_2O produced from different processes has distinctive preferential cleavages of $^{14/15}N$-^{16}O bond in their symmetric intermediates, which thus generates different intramolecular enrichments of $^{15}N^{\alpha}$ (^{14}N-^{15}N-^{16}O) or $^{15}N^{\beta}$ (^{15}N-^{14}N-^{16}O) in N_2O and leads to the distinct site preference (SP; Mothapo et al., 2015; Toyoda et al., 2002; Yu et al., 2020). Generally, bacterial denitrification possesses lower SP and $\delta^{18}O$ values of N_2O, whereas fungal denitrification has higher ones (Sutka et al., 2006, 2008; Toyoda et al., 2017; Zou et al., 2014). The SP value coupled with $\delta^{18}O$ of N_2O can differentiate N_2O sources among diverse processes (Rohe et al., 2017).

In this study, the isotope ratios of N_2O isotopocules ($\delta^{15}N^{\alpha}$ and $\delta^{15}N^{\beta}$) were measured by a gas chromatography–isotope ratio mass spectrometer (GC-IRMS). Additionally, streptomycin (STP) and cycloheximide (CYH) were used to inhibit bacterial and fungal respiration activities in the estuarine sediments, respectively (Maeda et al., 2017). We first explored the impacts of acidification on N transformations during biotic and abiotic denitrification in anoxic estuarine sediments using a N_2O isotopocules analysis combined with different inhibition strategies of bacteria or fungi. Then the relative contributions of denitrification-based N_2O production pathways under acidified and neutral conditions were estimated. Furthermore, the molecular mechanisms of acidification affecting bacterial and fungal denitrification were revealed, including the identification of denitrifiers keystone taxa and the exploration of electron transfer behaviors during denitrification and N_2O emission.

2 | MATERIALS AND METHODS

2.1 | Sampling and incubation experiments

In total, nine sediment cores were taken from three sampling sites of an estuary in Xiamen, China, in July 2019 (Figure S1), where heavy human activities may have recently released pollutants such as N into the waters. Estuarine sediments (10 kg) were collected with a gravity-corer (at 5.4 m, XDB-0205, ZX Co.), and the 10–50 cm overlying water (30 L) was sampled using a polymethyl–methacrylate sampler (FSS89-2500, Haifuda). The dissolved oxygen concentration of overlying water was measured in situ (0.05–0.11 mg/L, anoxic conditions) with a Water Quality Profiler (Hydrolab-DS5, HACH). At each of the three sampling sites, three sediment cores were collected

randomly as subsamples and then mixed to reduce sampling errors. The sediment and water samples were immediately sent back to the laboratory. After homogeneous mixing, the characteristics of sediments and water were analyzed as described by Su et al. (2019a).

pH-based acidification experiments were carried out during a 50-day anaerobic incubation and a subsequent 60-hr denitrification experiment as follows:

a. *Experiment 1 (50-day anaerobic incubation).* During the incubation, four pH levels were established as pH 5.0 (extreme conditions), 5.8 (after 3 centuries; Joint et al., 2011), 6.8 (background level), and 7.5 (common in the literature; Lee et al., 2019). Each pH level contained 200 g of estuarine sediments and 400mL of overlying water in a 1000-ml conical flask. Overlying water was adjusted by HCl or NaOH to reach the corresponding pH levels, and the headspace was purged with helium gas (99.99%) to keep in situ anoxic conditions. Then sediments were incubated in a temperature-controlled chamber (HWS-250) at 19°C for 50 days. During this period, fresh and pH-adjusted overlying water was supplemented to replace the existing water every 4 days to keep in situ environmental conditions. After each replacement, anoxic conditions also remained by aerating He for 10 min. Except for pH, other incubation conditions were similar to the in situ estuarine environments (details shown in Table S1), and microbial communities and activities were stable after 50 days (Su et al., 2021).
b. *Experiment 2 (60-h denitrification experiment).* To test the impacts of acidification on sedimentary denitrification and N_2O production, a subsequent 60-h denitrification experiment was conducted (refer Figure S2 for experimental design). We sampled sediments from each pH level after 50 days and established four incubation groups: (1) Control group, without any inhibitor; (2) bacterial inhibitor streptomycin (STP, fungal denitrification) group; (3) fungal inhibitor cycloheximide (CYH, bacterial denitrification) group; and (4) STP + CYH group (chemo-denitrification). STP can inhibit bacterial protein synthesis by disturbing peptidyl transferase at the 30S ribosomal subunit, and CYH can inhibit fungal protein synthesis by impeding translocation in elongation (Maeda et al., 2017). Concentrations of bacterial (STP, 6 mg g^{-1}) and fungal (CYH, 10 mg g^{-1}) inhibitors were determined by measuring the respiration inhibition ratio (≈1) (SI 2.1). Each group contained the four pH levels in triplicate. Each treatment contained 20 g of estuarine sediments and 40 ml of deionized water. Thereafter, water pH was adjusted by HCl solution to pH 5.0 (150 μl) and 5.8 (90 μl), and by NaOH to pH 7.5 (60 μl). To supply nitrogen and carbon sources, $NaNO_3$ and glucose were added to reach 1 mM nitrogen and 5 mM carbon (simulating urban and agricultural nonpoint pollution (Cheung et al., 2021)). Headspace was purged with helium gas. All treatments were then incubated at 25°C for 60 h. Liquid or gas samples were taken with 1-ml syringes. Concentrations of N and iron species including NO_3^-, NO_2^-, NH_4^+, N_2O, and N_2, as well as Fe^{2+} and Fe^{3+} concentrations were measured at 4- or 8-h intervals. After 60hr, N_2O and N_2 production rates, N_2O isotopocules, bacterial and fungal denitrifier communities, electron transfer efficiency, and functional gene abundances were analyzed. Detailed methods are provided in SI (S2.2 and S2.3) and the following sections.

2.2 | Isotope measurements and oxygen exchange

After the 60-h experiment, 12 ml of headspace gas from each treatment was collected and stored in pre-evacuated vials (Exetainer, Labco). N_2O isotopocules were analyzed using an isotope ratio mass spectrometer (IRMS, Delta V plus, Thermo) coupled to a preconcentrator system (Precon + Gasbench, Thermo; Rohe et al., 2017). Details are listed in SI S2.3. Values of N_2O isotopocules were determined by measuring the molecular N_2O^+ (*m/z*: 44/45/46) and the fragment NO^+ (*m/z*: 30/31). Pure N_2O (99.995%) whose isotopocules values have been analyzed in the laboratory of Thünen Institute of Climate-Smart Agriculture was used as internal reference gases. Two standards kindly offered by Dr. Reinhard Well and Anette Giesemann (Thünen Institute of Climate-Smart Agriculture, Germany) were used for performing two-point calibration for site preference (SP) values.

The isotope ratios of $^{15}N^{bulk}$, ^{18}O, $^{15}N^{\alpha}$, and $^{15}N^{\beta}$ of N_2O were determined using the following relationships:

$$\delta^{15}N^{i}(‰) = \left({}^{15}N^{i}_{sample} / {}^{15}N_{standard} - 1\right) (i = bulk, \alpha, or \beta), \quad (1)$$

$$\delta^{18}O(‰) = {}^{18}O_{sample} / {}^{18}O_{standard} - 1, \quad (2)$$

$$\delta^{15}N^{bulk}(‰) = \left(\delta^{15}N^{\alpha} + \delta^{15}N^{\beta}\right)/2, \quad (3)$$

where $^{15}N^{i}$ and ^{18}O, respectively, denote the isotope ratios of $^{15}N/^{14}N$ and $^{18}O/^{16}O$. $^{15}N^{\alpha}$ and $^{15}N^{\beta}$ are the ratios of $^{15}N/^{14}N$ at the center (^{14}N-^{15}N-^{16}O) and the edge (^{15}N-^{14}N-^{16}O) sites in the N_2O molecule, respectively. These ratios were presented as ‰ relative to Vienna Standard Mean Ocean Water (^{18}O) or atmospheric N_2 (^{15}N). The SP value of N_2O was determined as

$$N_2O\,SP(‰) = \delta^{15}N^{\alpha} - \delta^{15}N^{\beta}. \quad (4)$$

The typical measurement precisions are 0.3‰, 0.9‰, 0.9‰, and 0.6‰ for $\delta^{15}N^{bulk}$, $\delta^{15}N^{\alpha}$, $\delta^{15}N^{\beta}$, and $\delta^{18}O$, respectively.

$\delta^{15}N$ (−1.2 ± 2.3‰) and $\delta^{18}O$ (15.6 ± 0.8‰) of initial ^{15}N-NO_3^- and $\delta^{18}O$ (0.2 ± 0.1‰) of H_2O were measured according to Rohe et al. (2017).

During denitrification, the exchange of ^{18}O-N_2O with ^{18}O-H_2O would affect the actual $\delta^{18}O$ value of N_2O; thus, the $\delta^{18}O$-N_2O analysis could not be directly used to differentiate the N_2O sources (Rohe et al., 2017). In this study, we respectively applied two abundances of $\delta^{18}O$-H_2O (pure water from the lab: 0.2 ± 0.1‰ (natural abundance); from Aladdin: 32.5 ± 2.2‰ (10% ^{18}O atom)) to assess oxygen exchange during denitrification at each pH level. Oxygen exchange was corrected by the intercept of linear regression of the

$\delta^{18}O\text{-}N_2O/NO_3^-$ versus the $\delta^{18}O\text{-}H_2O/NO_3^-$ values (Equations 5 and 6; Rohe et al., 2017):

$$\delta^{18}O - N_2O/NO_3^- = {}^{18}O_{N_2O}/{}^{18}O_{NO_3^-} - 1, \quad (5)$$

$$\delta^{18}O - H_2O/NO_3^- = {}^{18}O_{H_2O}/{}^{18}O_{NO_3^-} - 1, \quad (6)$$

where ${}^{18}O_{N_2O}$, ${}^{18}O_{NO_3^-}$, and ${}^{18}O_{H_2O}$ denote the isotope ratios of ${}^{18}O/{}^{16}O$ of N_2O, NO_3^-, and H_2O, respectively. The intercepts at each pH level are shown in Table S2. The $\delta^{18}O\text{-}N_2O$ used in the following estimations is the corrected $\delta^{18}O$ of N_2O.

2.3 | N_2O isotope mass balance and error propagation

N_2O isotope mass balance was established to estimate the relative contributions of N_2O productions in the estuarine sediments between acidified and neutral conditions (Wankel et al., 2017). As the incubations were simulated under anoxic conditions, we only considered N_2O production from denitrification sources, including bacterial, fungal, and chemo-denitrification. Fractional contributions of the three processes to the total production of N_2O were expressed as

$$\text{Total } N_2O \text{ production} = f_B + f_F + f_C = 1, \quad (7)$$

where f_B, f_F, and f_C represent the fractional contributions of bacterial denitrification, fungal denitrification, and chemo-denitrification, respectively.

For SP values of N_2O production, isotope mass balance contributions of the three processes to the SP of N_2O production were expressed as

$$SP_p = f_B \times SP_B + f_F \times SP_F + f_C \times SP_C, \quad (8)$$

where SP_p denotes the SP values of N_2O before reduction (not the measured SP values). SP_B, SP_F, and SP_C represent the SP values for bacterial denitrification (−7.5–3.7‰, **0** ± 2.3‰), fungal denitrification (30.2·39.3‰, **37** ± 3.2‰), and chemo-denitrification (10–22‰, **16** ± 4.1‰), respectively (Table S3). The ranges of SP values for the three denitrification processes are summarized according to previous studies (Baggs, 2008; Decock & Six, 2013; Hu et al., 2015; Humbert et al., 2020; Jones et al., 2015; Sutka et al., 2008; Wankel et al., 2017; Yu et al., 2020; Zou et al., 2014). The mean values and standard errors for SP were obtained by estimating error propagation using the Monte Carlo sampling method in MATLAB and then were adjusted based on previous studies (Wankel et al., 2017; Zou et al., 2014).

Similar to SP values, the fractional contributions of the three processes to $\delta^{18}O$ of N_2O production were expressed as

$$\delta^{18}O_p = f_B \times \delta^{18}O_B + f_F \times \delta^{18}O_F + f_C \times \delta^{18}O_C, \quad (9)$$

where $\delta^{18}O_p$ denotes the $\delta^{18}O$ values of N_2O before reduction (not the measured $\delta^{18}O$ values). $\delta^{18}O_B$, $\delta^{18}O_F$, and $\delta^{18}O_C$ represent the $\delta^{18}O$ value for bacterial denitrification (17.4–26.5‰, **19** ± 3.6‰), fungal denitrification (30.2–51.9‰, **45** ± 10.8‰), and chemo-denitrification (24.3–36.5‰, **10** ± 6.3‰), respectively (Baggs, 2008; Frame & Casciotti, 2010; Hu et al., 2015; Humbert et al., 2020; Jones et al., 2015; Maeda et al., 2017; Sutka et al., 2006, 2008; Yu et al., 2020; Table S3). The mean values of SP and $\delta^{18}O$ estimated by the Monte Carlo method were the most appropriate for this study and used in the mass balance model (Wankel et al., 2017).

It is known that the SP and $\delta^{18}O$ values of residual N_2O will increase if N_2O reduction occurs such as bacterial denitrification. We suggested that N_2O reduction would occur before the mixing of N_2O produced from bacterial, fungal, and chemo-denitrification in estuarine sediments (Zou et al., 2014). Thus, the variations in SP and $\delta^{18}O$ values during N_2O reduction were assessed as

$$SP = SP_p - f_R \times SP\varepsilon_{N_2O}, \quad (10)$$

$$\delta^{18}O = \delta^{18}O_p - f_R \times \delta^{18}O\varepsilon_{N_2O}, \quad (11)$$

where SP and $\delta^{18}O$ represent the measured SP and $\delta^{18}O$ values of residual N_2O after reduction, respectively. f_R is the N_2O reduction degree and equals the proportion of the reduced (measured without C_2H_2) to total N_2O (measured with C_2H_2) concentrations. $SP_{\varepsilon N_2O}$ and $\delta^{18}O\varepsilon_{N_2O}$ are the kinetic isotope effect on SP (−6‰) and $\delta^{18}O$ (−25‰) (Ostrom et al., 2007) during N_2O reduction. Considering N_2O reduction during the incubation experiment (Equations 10 and 11), Equations (8) and (9) were modified as

$$SP = f_B \times SP_B + f_F \times SP_F + f_C \times SP_C - f_R \times SP\varepsilon_{N_2O}, \quad (12)$$

$$\delta^{18}O = f_B \times \delta^{18}O_B + f_F \times \delta^{18}O_F + f_C \times \delta^{18}O_C - f_R \times \delta^{18}O\varepsilon_{N_2O}. \quad (13)$$

Combining Equations (7), (12), and (13), we could estimate the relative contributions (f_B, f_F, f_C) of N_2O production from bacterial, fungal, and chemo-denitrification in the core incubations.

2.4 | Kinetics of chemo-denitrification process

Similar to the STP + CYH group (Section 2.1), 20 g of sediments was collected after the 50-day anaerobic incubation. Prior to pH adjustment with HCl or NaOH, 6 mg g^{-1} of bacterial inhibitor STP and 10 mg g^{-1} of fungal inhibitor CYH were added to the estuarine sediments. Subsequently, 1 mM $NaNO_3$ and 5 mM glucose were added, and the headspace was purged with helium gas. Each pH level was established in triplicate and then incubated at 25°C for 60 h. Concentrations of Fe species (Fe^{2+} and Fe^{3+}) and N species (NO_3^-, NO_2^-, N_2O, and N_2,) were measured at 0, 12, 36, and 60 h.

We applied a first-order kinetic model to evaluate the kinetics of the chemo-denitrification process in the estuarine sediments (Jones et al., 2015). The apparent first-order rates of NO_3^- and Fe^{2+} during chemo-denitrification were expressed as

$$\frac{d[NO_3^-]}{dt} = -K_{app1} \times [NO_3^-], \quad (14)$$

$$\frac{d[Fe^{2+}]}{dt} = -K_{app2} \times [Fe^{2+}], \quad (15)$$

where $[NO_3^-]$ and $[Fe^{2+}]$ were the concentrations of NO_3^- and Fe^{2+} during chemo-denitrification at each pH level, respectively. K_{app1} and K_{app2} denote the apparent rate constants of the variations in Fe^{2+} and NO_3^- concentrations during chemo-denitrification at each pH level, respectively. This apparent rate constant can reflect the level and rate of chemo-denitrification (Jones et al., 2015). K_{app1} and K_{app2} were determined by Equations (14) and (15), using the slopes of linear fittings of $\ln[NO_3^-]$ or $\ln[Fe^{2+}]$ with time at 0, 12, 36, and 60 h at each pH level.

2.5 | Electron transfer efficiency

Behaviors of electron transfer during denitrification process greatly influence bacterial and fungal N_2O metabolisms (Su et al., 2019a; Zumft, 1997). Electron transfer efficiency was thus measured in this study through an electron respiration approach by reducing tetrazolium chloride to formazan (Broberg, 1985; Wan et al., 2016). After incubation, 5 g of estuarine sediments were collected from the STP and CYH groups. Sediments were first washed with 4°C 0.05 M phosphate-buffered saline (PBS) thrice at 4500 rpm for 10 min and then resuspended in PBS. One milliliter 0.5% tetrazolium chloride and 1 mg NADH were added into the resuspended sediment. After incubation in the dark for 30 min (25°C), 1-ml formaldehyde (HCHO) was injected into the sediment to terminate the reaction. The supernatant of the mixture was removed by centrifuging at 4500 rpm for 10 min. Then, 5-ml 96% methanol was added into the sediment to extract formazan at 200 rpm for 30 min. The supernatant was collected after being centrifuged at 10,000 rpm for 5 min. Absorbance of the generated orange-like supernatant was quantified at 490 nm. The electron transfer efficiency was estimated as

$$\text{Electron transfer efficiency}\left(\mu g\, O_2\, min^{-1}\, g^{-1}\, \text{sediments}\right) = \frac{ABS_{490}}{15.9}\frac{V}{V_0 t}\frac{32}{2}\frac{1}{m}, \quad (16)$$

where ABS_{490} is the absorbance of the supernatant at 490 nm; 15.9 is the absorptivity of tetrazolium chloride–formazan; V_0 and V (ml) are the volumes of initial mixture and methanol, respectively; t (min) is the incubation time; 32/2 is the factor for the transformation of tetrazolium chloride–formazan to O_2; and m (g) is the sediment mass.

2.6 | Bacterial and fungal genetic sequencing

After the 60-h experiment, 3.5 g of estuarine sediments from each pH treatment of Control, STP, and CYH groups were collected. Genomic DNA was extracted using a Power Soil DNA Isolation Kit (MoBio) according to the instructions. 16S rRNA gene (for the bacterial community), bacterial *nirS* gene (for the *nirS*-type bacterial denitrifier), bacterial *nirK* gene (for the *nirK*-type bacterial denitrifier), ITS gene (for the fungal community), and fungal *nirK* gene (for the *nirK*-type fungal denitrifier) were amplified with the primer sets 515F/907R, cd3aF/R3cd, F1aCu/R3Cu, ITS1F/ITS2R, and EunirK-F1/EunirK-R2, respectively (Table S4). Identification of fungal denitrifier communities in the estuarine sediments was based on the EunirK-F1/EunirK-R2 and ITS1F/ITS2R primers according to previous studies (Maeda et al., 2015; Mothapo et al., 2015). PCR products were purified by a DNA purification kit (DP214-3, Tiangen) and were pooled for library constructions. Pooled samples were sequenced at the Illumina MiSeq platform. Raw sequences were quality filtered, chimera checking and grouped at the 97% sequence similarity (Caporaso et al., 2010). Taxonomy was assigned by comparison to Silva (16S rRNA gene), GenBank (functional gene), and UNITE (ITS gene) databases with QIIME. Community phylogenetic investigation by the reconstruction of unobserved-states (PICRUSt)-based predictions was conducted as described by Douglas et al. (2020) and Langille et al. (2013). Accession number is SUB8289327.

The PCR conditions for fungal-denitrifying gene *nirK* included the initial heating at 94°C for 10 min, followed by 40 cycles at 94°C for 60 s, annealing for 30 s at 53°C, and extension for 60 s at 72°C (Table S4; Maeda et al., 2015). Bacterial-denitrifying genes (i.e., *napA*, *narG*, *nirS*, *nirK*, and *nosZ*; Table S5) were quantified by the qPCR-based SmartChip technique according to our previous study (Zheng et al., 2018). Briefly, 3.1 μl of DNA, 24.8 μl of Mix-enzyme, and 3.1 μl of gene primers were added to a SmartChip, which was then detected by a SmartChip PCR system (WaferGen, Biosystems). We used 16S rRNA gene as a reference gene. The qPCR conditions were initial heating at 95°C for 10 min, followed by 40 cycles at 95°C for 30 s, annealing for 30 s at 58°C, and extension for 30 s at 72°C. Samples with the threshold cycle C_T less than 31 were selected for downstream analysis (Chen, Ding, et al., 2020; Zheng et al., 2018). These genes were regarded to be detected when they were targeted in all three replicates. Relative copy numbers of 16S rRNA gene and functional gene are as follows (Zheng et al., 2018):

$$\text{Relative copy number of gene} = 10^{(31-C_T)/(3.33)}. \quad (17)$$

Normalized relative abundance of functional genes is the proportion of the relative copy number of the functional gene to that of 16S rRNA gene, which was used as the reference gene (Zheng et al., 2018):

$$\text{Normalized relative abundance of functional gene} = \text{Relative copy number of functional gene}/\text{relative copy number of 16S gene}. \quad (18)$$

2.7 | Statistical analysis

Prior to the statistical test, the Shapiro–Wilks analysis was applied for the normality test. The data fitted normal distribution. The impacts of acidification on Fe concentrations, N_2O/N_2 production rates, N_2O isotope abundances, electron transfer efficiency, electron transfer

protein reads, and functional gene abundances were statistically examined using one-way ANOVA followed by a post-hoc Tukey test ($p < .05$) in IBM SPSS (version 22.0). Alpha-diversity was calculated by R. Permutational multivariate analysis of variance (PERMANOVA) was applied to evaluate the impacts of acidification on denitrifying community dissimilarity (Bray–Curtis distance). Pearson correlation was conducted among *nirS*-type and *nirK*-type bacterial denitrifiers and *nirK*-type fungal denitrifiers, in which nodes ($r^2 > .9$ and $p < .05$) were selected for network analysis. Co-occurrence network analysis of bacterial and fungal denitrifiers was presented by Gephi software (v0.9.2).

3 | RESULTS

3.1 | N transformation and balance

Transformation and balance of N speciation in each group under different pH levels showed a striking heterogeneity (Figure 1; Figure S3). In the Control group and CYH (bacterial denitrification) group, acidification inhibited reductions of NO_3^- and NO_2^- by 5%–17% (pH 5.0) and 10%–59% (pH 5.8), respectively (Tukey, $p < .05$) and reduced the production rates of N_2 in the estuarine sediments compared with those at pH 6.8 and 7.5 ($p < .05$, Figure 1a,b; Figure S4). It is worth mentioning that acidification stimulated N_2O emissions significantly ($p < .01$) in the Control and CYH groups by 223%–438% upon the termination of incubation (Figure 1; Figure S3). For the STP group (fungal denitrification), NO_3^- reduction was also inhibited by acidification, but the reduction rate was lower than that in the Control and CYH groups ($p < .01$, Figure 1a). This is because fungal denitrification commonly starts with NO_2^- reduction, owing to the uncommon dissimilatory NO_3^- reductase in most fungal denitrifiers (Kobayashi et al., 1996; Uchimura et al., 2002). Furthermore, as fungal denitrifiers lack N_2O reductase (catalyzing N_2O to N_2; Kobayashi et al., 1996; Shoun & Tanimoto, 1991), the emissions of N_2O increased with incubation time and much less N_2 production was detected in the STP group (Figure 1c,d). In addition, NH_4^+ levels in all groups were enhanced with incubation time although acidification suppressed its increasing rate (Figure 1e), suggesting that dissimilatory NO_3^- reduction to NH_4^+ may also occur in the estuarine

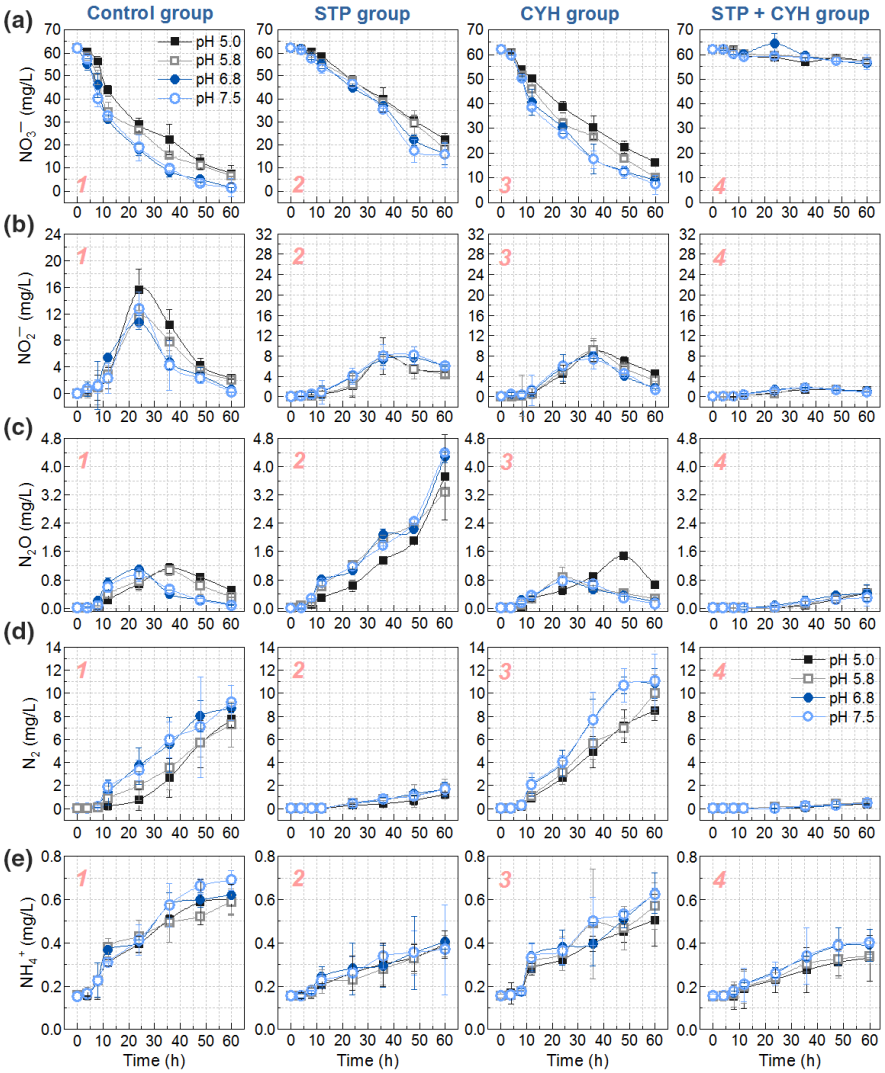

FIGURE 1 Acidification responses of N speciation in the estuarine sediments along with time. (a) Nitrate. (b) Nitrite. (c) Nitrous oxide. (d) Dinitrogen gas. (e) Ammonium. *1* is the Control group without any inhibitor. *2* is the STP group with bacterial inhibitor streptomycin. *3* is the CYH group with fungal inhibitor cycloheximide. *4* is the STP + CYH group with both bacterial and fungal inhibitors. Error bars mean the standard deviation ($n = 3$)

sediments (Wang, Pi, Song, et al., 2020), and its rate is likely higher than that of the potential anammox process which consumes NH_4^+ in the estuarine sediments.

Bacteria and fungi in the STP + CYH group were expected to be inactivated due to applications of inhibitors; however, we still observed a slight NH_4^+ increase, NO_2^- reduction, and N_2O yield in all pH treatments (Figure 1b,c,e). One possible reason was insufficient inhibitions of STP and CYH (Mothapo et al., 2015). For instance, STP has been reported to inactivate only 60%–70% of total bacterial respiration in soil environments (Velvis, 1997). The survived denitrifiers could be involved in NH_4^+ increase, NO_2^- reduction, and N_2O emission. On the other hand, abiotic pathways in anoxic sediments such as chemo-denitrification (i.e., iron-Fe^{2+} and NO_3^-/NO_2^-) can also contribute to the emission of N_2O (Samarkin et al., 2010). For example, sediment surface-bound reduced iron-Fe^{2+} can act as an available activator for NO_3^- or NO_2^- reduction and subsequent N_2O production (Samarkin et al., 2010; Wankel et al., 2017). Although the traditional respiration inhibition approach can distinguish the dominant N_2O sources from bacteria and fungi and even from chemical sources (Mothapo et al., 2015), the accuracy of assessments from this approach is still in question. To solve the problem, N_2O isotopocules analysis was employed to estimate the relative contributions of N_2O emission from the three candidate processes at each pH level.

3.2 | Multi-isotope analysis of N_2O emission processes

The stable isotopic compositions of N_2O, including $\delta^{15}N^{bulk}$, $\delta^{15}N^{\alpha}$, $\delta^{15}N^{\beta}$, and $\delta^{18}O$, as well as the intramolecular SP ($^{15}N^{\alpha}$-$^{15}N^{\beta}$), provided better insights into biogeochemical mechanisms governing sedimentary N_2O production and reduction under acidified and neutral conditions (Figure 2a; Figure S5). SP analysis of N_2O has been widely used to distinguish N_2O dynamics from bacterial (lower SP values) and fungal (higher SP values) sources, based on the different fractionation mechanisms of $^{15}N^{\alpha}$ and $^{15}N^{\beta}$ during nitric oxide (NO) reduction (Figure 2b; Yu et al., 2020). Bacterial NO reductase, holding a binuclear center, simultaneously binds two N atoms of NO molecules to engender an intermediate hyponitrite (ON-NO) prior to forming N_2O (Figure 2b; Watmough et al., 2009). The two N atoms in ON-NO have little isotopic preference, thus producing a low SP value. In contrast, fungal NO reductase P450nor has only one catalytic center (Figure 2b; Toyoda et al., 2017), and the first and second N atoms sequentially stay at the β and α positions of N_2O molecules, respectively (Toyoda et al., 2017). As isotopically lighter ^{14}N reacts faster than the heavier ^{15}N (Fry, 2006), fungal denitrification favors more enrichments of $^{15}N^{\alpha}$ than $^{15}N^{\beta}$ in N_2O molecules, therefore generating a higher SP value. In this study, the average SP values in the STP and CYH groups were 25.72–40.70‰ and 1.73–17.25‰, respectively (Figure 2a; Figure S5), similar to previously reported fungal denitrification (30.2–39.3‰; Lewicka-Szczebak et al., 2017; Sutka et al., 2008; Zou et al., 2014) and bacterial denitrification (−7.5–3.7‰; Sutka et al., 2006; Toyoda et al., 2017; Yu et al., 2020; Zou et al., 2014). In the Control group, the average SP of N_2O at pH 6.8 and 7.5 was significantly ($p < .01$) higher than that at pH 5.0 and 5.8 (Figure 2a; Figure S5), suggesting that acidification may change the pathways of N_2O production in the estuarine sediments.

The mixing model of N_2O isotope using SP analysis alone cannot quantify N_2O production when considering three or more end members (Duan et al., 2017; Fry, 2006). The $\delta^{18}O$ isotope signature of N_2O is another promising tool to identify different sources of N_2O (Lewicka-Szczebak et al., 2017; Maeda et al., 2017). Coupling $\delta^{18}O$ with the SP of N_2O, we established a multi-isotope mass balance to identify the relative contributions of N_2O productions from the three end members of bacterial, fungal, and chemo-denitrification. Meanwhile, N_2O reduction during bacterial denitrification and oxygen exchange with H_2O was also considered (Section 2.3). In this study, the semi-quantitative mass balance revealed that acidification altered the relative contributions of sedimentary N_2O production from the three sources (Figure 2c). In pH 6.8 and 7.5 of the Control group, fungal denitrification was dominant in N_2O production, contributing 41%–69% of total N_2O production ($p < .001$, Figure 2c). In contrast, bacterial denitrification became dominant at pH 5.0 and 5.8 levels and released 37%–56% of total N_2O ($p < .01$, Figure 2c).

Under natural conditions, it was previously thought that N_2O emission from sediments could mainly be derived from bacterial denitrification (Gao et al., 2020; Wang, Pi, Jiang, et al., 2020). However, our study indicated that the fungal source was dominant under background conditions (pH 6.8 and 7.5), which is also similar to the observation that fungal N_2O production might not be overlooked in coastal environments (Wankel et al., 2017). This is likely because activities of bacterial denitrifiers were unaffected under neutral conditions (pH 6.8 and 7.5) and thus could effectively reduce N_2O to N_2 (Figure 1d). By contrast, fungal denitrifiers could not perform N_2O reduction due to lack of N_2O reductase, thereby resulting in fungal N_2O emission and its preponderance. In soil ecosystems, N_2O production from fungi was also nearly one order of magnitude higher than that from bacterial denitrifiers, even though the abundance of fungal denitrifiers was lower than that of bacterial denitrifiers (Laughlin & Stevens, 2002). Our findings may indicate that fungal denitrification could have great influences on N_2O emission in estuarine ecosystems, acting as an important but previously underestimated source. Therefore, the role of fungi in N_2O emissions should not be ignored in future studies. However, under acidified conditions (pH 5.0 and 5.8), N_2O production predominantly switched to a bacterial source (Figure 2c). Because bacterial N_2O emission (CYH group) was significantly increased by acidification and the fungal source (STP group) decreased ($p < .01$, Figure 1c), bacterial denitrification became the major source. With global ocean acidification increasing rapidly, such an increase in bacterial N_2O yield could influence climate change in global estuarine regions. These results also highlight that acidification effects should be considered when estimating N_2O fluxes in estuarine ecosystems in the future.

In addition to biotic pathways, the abiotic production of N_2O such as chemo-denitrification has also recently attracted some attention but its ecological role remains unclear (Jones et al., 2015;

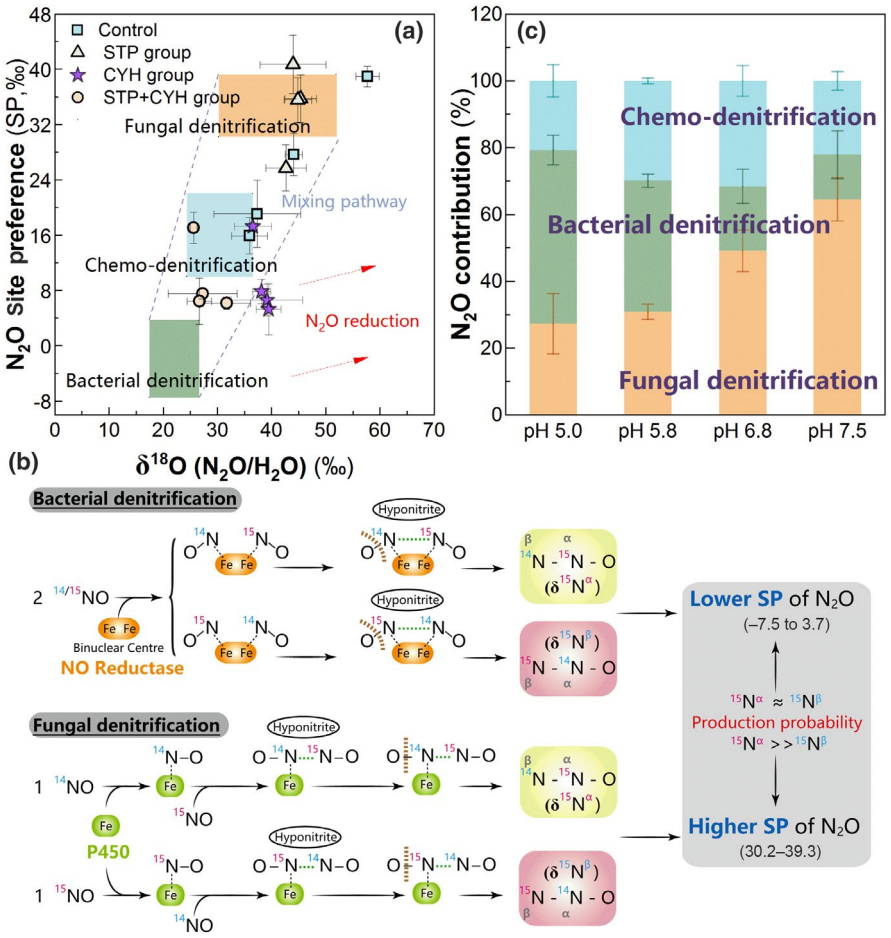

FIGURE 2 Acidification responses of multiple-isotope information of N_2O showing the relative contributions of N_2O productions from bacterial, fungal, and chemo-denitrification. (a) Relationships between N_2O SP and $\delta^{18}O$. This $\delta^{18}O$ value is corrected for the ^{18}O-N_2O exchange with ^{18}O-H_2O during denitrification (i.e., $\delta^{18}O$ (N_2O/H_2O)). Colored ranges represent the previously reported SP and $\delta^{18}O$ from bacterial (Sutka et al., 2006; Toyoda et al., 2017; Zou et al., 2014), fungal (Lewicka-Szczebak et al., 2017; Sutka et al., 2008), and chemo-denitrification (Jones et al., 2015; Wei et al., 2019; Yu et al., 2020), which is first used by Lewicka-Szczebak. The purple area denotes the N_2O mixing of the three anoxic processes, and the red arrow denotes the N_2O reduction by bacterial denitrification on the basis of earlier studies (slope ε (SP)/ε ($\delta^{18}O$) = 0.57). (b) Illustrations of bacterial and fungal NO reductions regulating the positions (central or edge) of ^{14}N and ^{15}N in the formation of N_2O (Duan et al., 2017; Toyoda et al., 2017). (c) Relative contributions of N_2O productions from bacterial, fungal, and chemo-denitrification at each pH level of the Control group. Errors were estimated by random sampling error propagation simulation

Laughlin & Stevens, 2002; Wei et al., 2019). Therefore, direct measurement of chemo-denitrification and model estimation with N_2O isotope mass balance were applied to investigate the chemo-denitrification in the estuarine sediments. Chemo-denitrification is a complex process primarily due to different mechanisms associated with various substrates such as hydroxylamine, NO_3^-, and NO_2^-, which can react with Fe^{2+} to produce N_2O (Heil et al., 2014; Toyoda et al., 2005). In this study, the incubations were conducted under anoxic conditions, and thus, the hydroxylamine from nitrification can be neglected. N_2O production from chemo-denitrification may be related to two reactions, which are Fe^{2+} and NO_3^- through $12Fe^{2+} + 2NO_3^- + 11H_2O \rightarrow 4Fe_3O_4 + N_2O + 22H^+$ ($\Delta G^0 = -509.6$ kJ mol^{-1}) and Fe^{2+} and NO_2^- through $6Fe^{2+} + 2NO_2^- + 5H_2O \rightarrow 2Fe_3O_4 + N_2O + 10H^+$ ($\Delta G^0 = -291.7$ kJ mol^{-1}; Jones et al., 2015; Samarkin et al., 2010). In the STP + CYH group, we found that concentrations of Fe^{2+} and NO_3^- in the estuarine sediments declined with incubation time, whereas Fe^{3+} and N_2O increased (Figure S6). This indicates that the chemo-denitrification process did occur in the estuarine sediments.

Furthermore, we used the first-order kinetic model and apparent rate constant K_{app} to examine the chemo-denitrification rate in response to acidification (Figure 3). The apparent rate constants K_{app} of NO_3^- and Fe^{2+} were 0.056–0.070 h^{-1} and 0.065–0.072 h^{-1}, respectively, lower than those in pure chemical reaction systems (0.11–0.15 h^{-1}; Jones et al., 2015). This implies that the chemo-denitrification process was slower in the estuarine sediments. No significant difference was observed in K_{app} among pH levels (Figure 3). Generally, the optimum pH level for the chemo-denitrification process (Fe^{2+} and NO_3^-) is ~8 (Chen, Yuan, et al., 2020; Wu et al., 2012) while our sediments were incubated at pH 5.0–7.5 (acidified and in situ estuarine conditions), which could have led to the reduced chemo-denitrification rate. N_2O isotope mass balance (Section 2.3) was further applied to estimate the relative contribution of N_2O

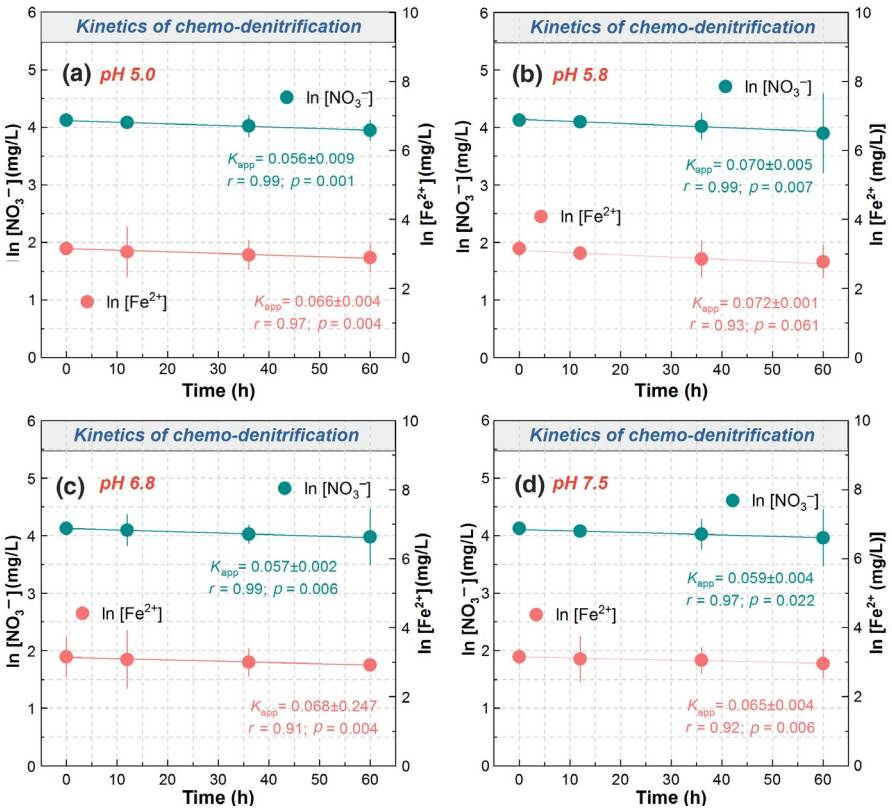

FIGURE 3 First-order kinetic model revealing Fe^{2+} and NO_3^- kinetics of the chemo-denitrification process at each pH level in the STP + CYH group. (a) pH 5.0; (b) pH 5.8; (c) pH 6.8; and (d) pH 7.5. K_{app} is the apparent rate constant of Fe^{2+} or NO_3^- during the chemo-denitrification process in the STP + CYH group. K_{app} is determined by the slope of the linear fitting of ln [Fe^{2+} (mg/L)] or ln [NO_3^- (mg/L)] with time at 0, 12, 36, and 60 h at each pH level. Green dots represent ln[NO_3^-]; red dots represent ln[Fe^{2+}]. Error bars mean the standard deviation ($n = 3$)

production from the chemo-denitrification process. Our results showed that despite the lack of effect from acidification, chemo-denitrification contributed up to 16%–35% of total N_2O production (Figure 2c), confirming the results from the direct measurement of chemo-denitrification. This suggests that the chemical source of N_2O production should be considered when estimating N_2O fluxes in estuarine ecosystems, although the rate of the process was relatively low. To verify the reliability of N_2O isotope mass balance, we used the data from the STP (fungal denitrification) group and CYH (bacterial denitrification) group to estimate and calibrate the prescribed $\delta^{18}O$ and SP values (Table S6). In the STP group, fungal N_2O was dominant (77.3%–88.0%), and in the CYH group, bacterial N_2O contributed 72.2%–81.7% of total N_2O production, both of which are consistent with the hypothesis of these two groups. Moreover, N_2O from chemo-denitrification of the two groups contributed 10.2%–21.6%, similar to that of the Control group. These observations indicated that estimates of the mass balance could be reliable. Although more precise contributions of the three endmembers changed with the prescribed $\delta^{18}O$ and SP values (Table S3), all ranges suggested that great contributions of N_2O productions from fungal and chemo-denitrification pathways cannot be ignored.

3.3 | Bacterial and fungal denitrifiers

Given that oxygen content, carbon source, and temperature were controlled, microbial community and functional gene abundances of denitrifiers could be the critical factors accounting for the acidification impacts on sedimentary denitrification and N_2O emission in this study. Information on fungal denitrifier community in aquatic ecosystems, especially in estuarine environments, is less investigated than in terrestrial ecosystems (Grossart et al., 2019). To better understand sedimentary denitrifiers in response to acidification, we characterized *nirS*-type and *nirK*-type denitrifiers (Figure 4; Table S7; Figure S7). Acidification significantly altered the community structures of *nirS*-type ($p = .001$), *nirK*-type ($p = .008$) bacterial denitrifiers, and *nirK*-type ($p = .008$) fungal denitrifiers in the estuarine sediments (Figure 4a–c) and reduced their α-diversity (Table S7). Sedimentary denitrifier compositions were also changed by acidification (Figure S7). Network analysis was applied to distinguish the variations of "core microbiome," also known as "keystone taxa" (Banerjee et al., 2018), of sedimentary denitrifiers in response to acidification (Figure 4d). Co-occurrence networks at each pH level revealed that acidification reduced the complexity of denitrifier networks, reflecting the weakened interactions between bacterial and fungal communities. More importantly, the key node compositions (keystone taxa of denitrifiers) were also changed (Figure 4d). Under acidified conditions (pH 5.0 and 5.8), *Azospirillum*, *Acidovorax* (*nirS*-type bacterial denitrifiers), *Rhizobium* (*nirK*-type bacterial denitrifiers), *Fusarium*, and *Aspergillus* (*nirK*-type fungal denitrifiers) were the keystone taxa and presented the most connections with other denitrifiers (Figure 4d). Of note, in addition to fungi, most of these keystone taxa of bacterial denitrifiers such as *Azospirillum* and *Acidovorax* are incomplete denitrifiers due to the absence of *nosZ* gene (encoding N_2O reductase; Vial et al., 2006; Zhong et al., 2009), partly explaining the accumulations of

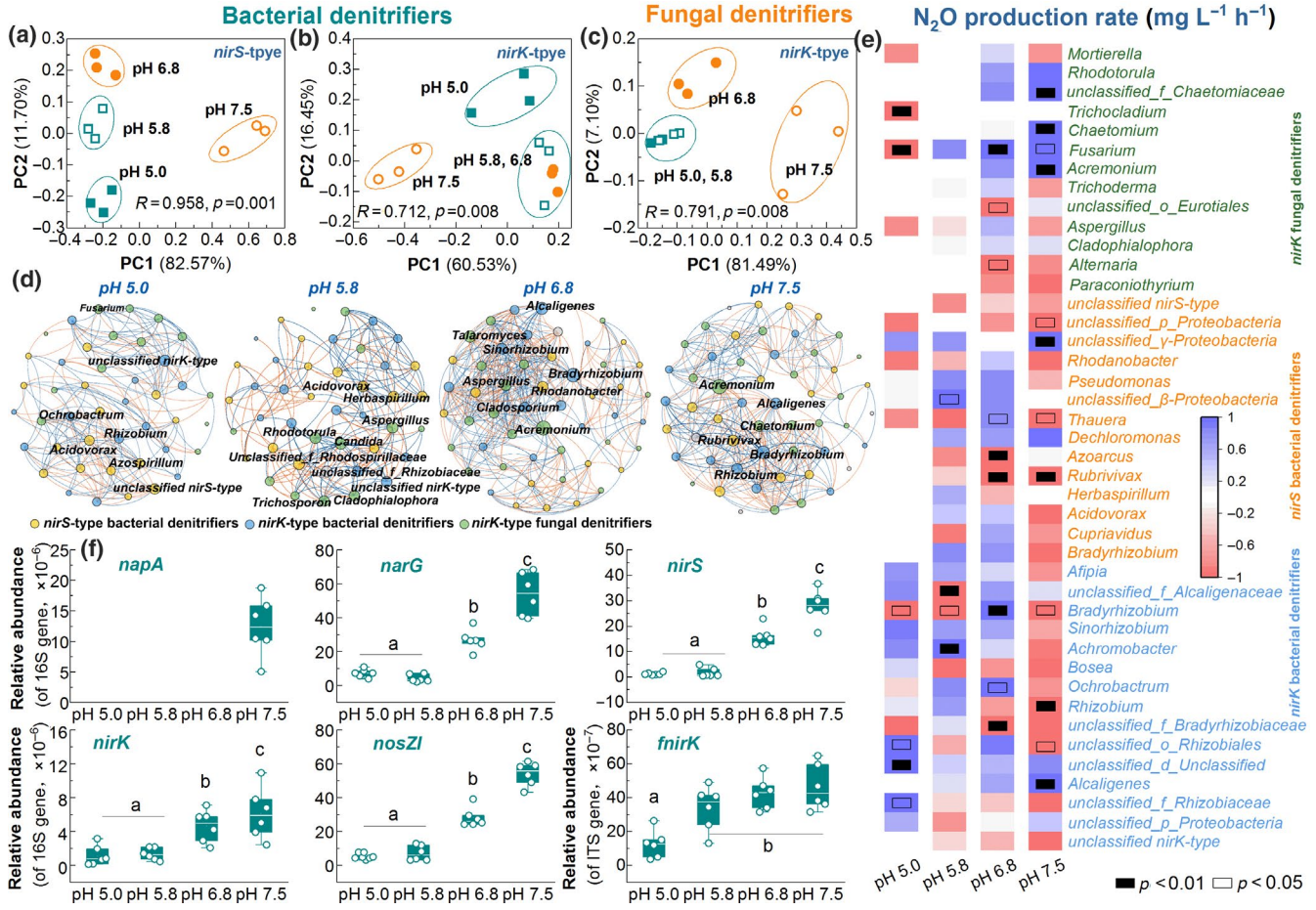

FIGURE 4 Characteristics of bacterial and fungal denitrifiers in the estuarine sediment in response to acidification. (a–c) Principal coordinates analysis (PCoA)–based Bray–Curtis distance showing the acidification impacts on the community structures of *nirS*-type and *nirK*-type bacterial denitrifiers, and *nirK*-type fungal denitrifiers. Fungal denitrifiers do not possess *nirS* gene. (d) Co-occurrence network analysis showing the shifts in keystone taxa of denitrifiers by acidification ($p < .05$ and $r^2 > .9$). (e) Correlations between relative abundances of denitrifiers and N_2O production rates at each pH level. (f) Relative abundances of denitrifying functional genes *napA*, *narG*, *nirS*, *nirK*, and *nosZ* in bacteria, and *nirK* in fungi. Different letters (a, b, c) represent the significant differences at each pH level ($n = 6$, Tukey, $p < .05$)

bacterial N_2O at pH 5.0 and 5.8 in this study (Figure 1c). Under neutral conditions (pH 6.8 and 7.5), however, the keystone taxa shifted to *Rubrivivax* (*nirS*-type bacterial denitrifiers), *Bradyrhizobium* (*nirK*-type fungal denitrifiers), and *Acremonium* (*nirK*-type fungal denitrifiers) (Figure 4d). These keystone taxa of bacterial denitrifiers (*Rubrivivax* and *Bradyrhizobium*) are complete denitrifiers and can reduce NO_3^- or NO_2^- to N_2, leading to less bacterial N_2O accumulation (Bedmar et al., 2005; Nagashima et al., 2012). The aforementioned findings indicated that the keystone taxa of bacterial denitrifiers were shifted from N_2O-reducing (complete denitrification) under neutral conditions to N_2O-producing (incomplete denitrification) under acidified conditions. This shift may partly explain the increased N_2O emission under acidified conditions, and the changed N_2O production pathways between acidified and neutral conditions in the estuarine sediments. Additionally, the significant correlations between denitrifier abundances and the potential production rates of N_2O further supported that the keystone taxa could likely affect N_2O emission in the estuarine sediments (Figure 4e).

Acidification also changed the abundances of sedimentary denitrifiers (Figure S7). At the phylum level, the abundance of Proteobacteria in the bacterial community was decreased, but the abundance of Ascomycota in the fungal community was increased. Moreover, the genera abundances of those keystone taxa were also altered by acidification (Figure S7). It is worth mentioning that the relative abundances of these keystone taxa were less than 0.5%, generally defined as "rare microbial taxa" (Lynch & Neufeld, 2015), with the exceptions of *Rhizobium* (1.9%) and *Bradyrhizobium* (1.3%). These observations highlighted the importance of rare taxa in mediating microbial denitrification. The role of rare taxa is increasingly recognized, owing to their capacities in estimating key functions and driving element cycling in aquatic and/or terrestrial ecosystems (Chen, Ding, et al., 2020; Lynch & Neufeld, 2015). They are more sensitive to environmental pressure compared to those abundant representatives and could offer more robust information on microbial communities and ecosystems. For example, Lynch and Neufeld (2015) and Chen, Ding, et al. (2020) reviewed that rare microbial

taxa could act as an important contributor to evaluate microbial diversity and reflect multifunction of soil ecosystems. Some recent studies also documented that distinctive phylogenetic features of microorganisms were associated with rare taxa members of bacterial and fungal communities, despite lacking direct evidence for the relationship between the abundance of rare taxa and phylogenetic novelty (Elshahed et al., 2008; Galand et al., 2009). As part of microbial seed banks, nearly 1.5%–28% of microorganisms are conditionally rare taxa and can become dominant under several conditions (Chen, Ding, et al., 2020), such as algal blooms or acidification (Lynch & Neufeld, 2015). Our results demonstrated that acidification affected rare keystone taxa of denitrifiers and may therefore change N_2O production pathways, indicating that rare-biosphere denitrifiers could exhibit disproportionately large influences on N cycling in estuarine sediments.

Denitrifying functional gene abundances were quantified at each pH level (Figure 4f). The bacterial gene *napA*-encoding periplasmic NO_3^- reductase was detected only at pH 7.5. The relative abundances of *narG* encoding membrane-bound NO_3^- reductase, *nirS*/*nirK* encoding NO_2^- reductase, and *nosZ* encoding N_2O reductase were all significantly reduced by acidification ($p < .05$). This probably explains the accumulations of NO_2^- and N_2O under acidified conditions at the end of the 60-h experiment. By comparison, the relative abundance of fungal *nirK* gene-encoding fungal NO_2^- reductase was decreased only at pH 5.0 ($p < .05$, Figure 4f).

3.4 | Electron transfer

Bacterial and fungal N_2O metabolisms are driven by the electron flows from donors to acceptors (Figure 5), and thus, the behaviors of electron transfer and consumption in denitrifiers greatly influence N_2O production and reduction (Su et al., 2019b; Wan et al., 2016). We found that acidification significantly affected electron transfers for both bacterial and fungal denitrification (Figure 5). Acidification decreased the efficiencies by 17%–54% and 11%–28% for bacterial and fungal denitrification, respectively ($p < .01$, Figure 5a,b). Moreover, three types of key electron transfer proteins (ETPs, such as NADH dehydrogenase, quinol-cyctochromebc1, and cytochrome *c*) were also inhibited ($p < .05$, Figure 5), regardless of bacterial and fungal denitrifiers. During N_2O emission, these ETPs are responsible for driving electron flows from organics or NADH to NO and N_2O reductases that subsequently consume the electrons to produce and reduce N_2O (Zumft, 1997). Therefore, the decreased electron

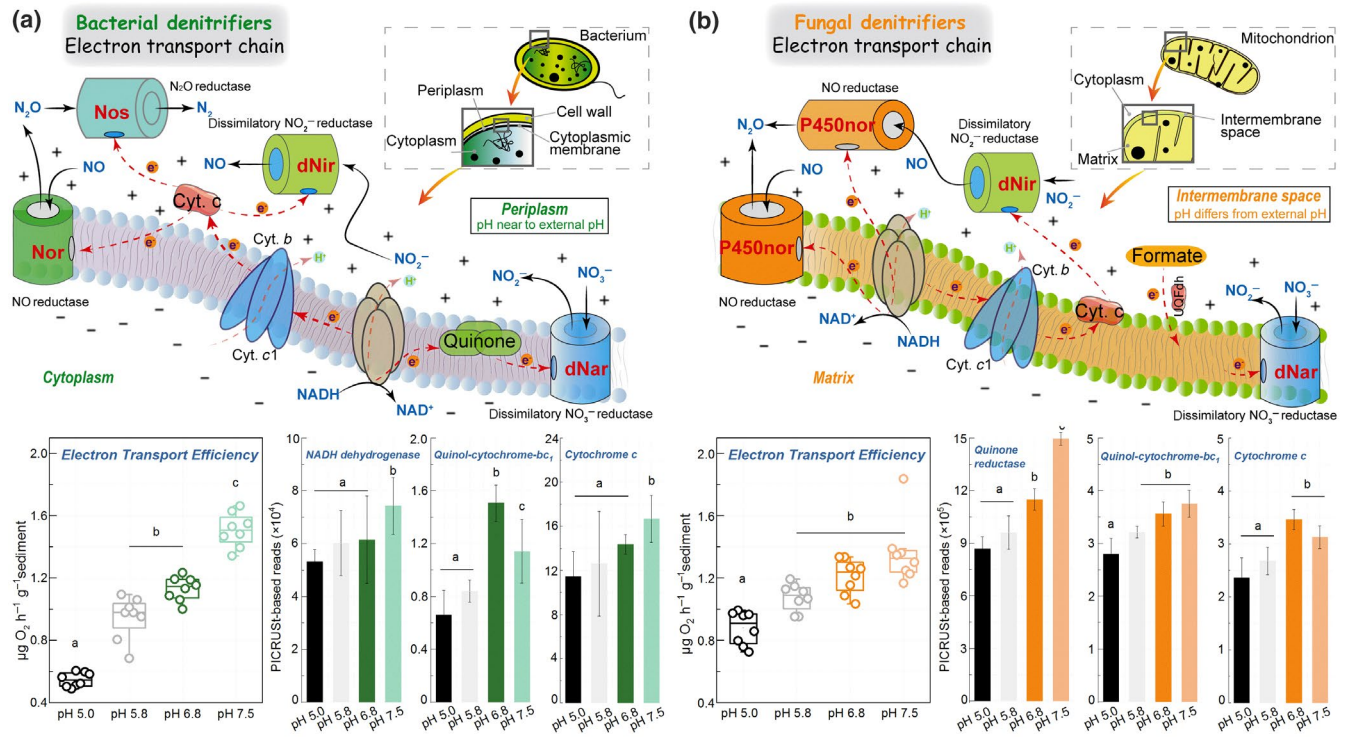

FIGURE 5 Electron transfers and consumptions during bacterial and fungal denitrification. Schematic representation of the electron transfer chain in bacterial (Zumft, 1997) (a) and fungal (Shoun et al., 2012) (b) denitrifiers. In bacterial denitrifiers, NADH is catalyzed by electron transfer protein NADH dehydrogenase to generate electrons. One flux of electrons is consumed by dissimilatory NO_3^- reductase (dNar), and the other flux is transferred to cytochrome c via quinol-cyctochromebc1 and then consumed by dissimilatory NO_2^-, NO, and N_2O reductases. In fungal denitrifiers, the distinctive NO reductase P450nor utilizes electrons directly from NADH to produce N_2O. Moreover, electrons consumed by dNar are directly derived from formate that is formed from pyruvate. Both bacterial and fungal electron transfer efficiencies ($n = 8$) were decreased by acidification. Three types of electron transfer protein reads based on PICRUSt analysis were decreased as well ($n = 3$). Different letters (a, b, c) represent the significant differences at each pH level (Tukey, $p < .05$)

transfer efficiency and the reduced ETPs abundances indicated that acidification directly disturbed bacterial and fungal electron transfer behaviors and then affected their N_2O emissions in the estuarine sediments. Some distinctive characteristics existed in denitrifying metabolic pathways between bacterial and fungal denitrifiers (Figure 5a,b). In bacterial denitrifiers, the electron transfer chain locates in the cytoplasmic membrane. The produced NADH is catalyzed by ETP (NADH dehydrogenase) to generate electrons that are then consumed by NO and N_2O reductases (Figure 5a; Li et al., 2016; Zumft, 1997). Importantly, unlike NO reductase (responsible for N_2O production), N_2O reductase (responsible for N_2O reduction) is distributed in the periplasm (Su et al., 2019a; Zumft, 1997), and its activity could be disrupted more easily than NO reductase under acidified conditions (Liu et al., 2010; Pan et al., 2012). This means that the effect of acidification on N_2O reduction is stronger than on N_2O production, explaining the increased bacterial N_2O emission at the end of the experiment under acidified conditions (pH 5.0 and 5.8, Figure 1c) and thus promoting the contribution of bacterial source (Figure 2c). For fungi, however, the electron transfer chain lies in the membrane of the mitochondrion in fungal denitrifiers (Figure 5b), which may be less likely affected by acidification compared to bacteria. Nonetheless, fungal electron transfer efficiency and the activity of distinctive NO reductase-P450nor were also reduced by acidification, leading to a decline in N_2O production under acidified conditions (Figure 1c) and thus decreasing the contribution of fungal denitrification to N_2O emission. These results explain the changes in the predominant pathways of N_2O production between acidified and neutral conditions (Figure 2c).

In addition, we also found that the impacts of acidification on the electron transfers of bacterial denitrifiers were more prominent than those of fungal representatives (Figure 5). Besides different locations of the electron transfer chain, some other alternative explanations could also account for this different response to acidification. It is generally accepted that the bacterial-denitrifying system is only dedicated to energy harvest, whereas the fungal-denitrifying system could be coupled with other metabolic pathways, such as detoxification (Mothapo et al., 2015). Moreover, fungal denitrifiers have strong adaptation and metabolic capacity in a wide range of environments, including acidic and alkaline conditions (Mothapo et al., 2015). These further explain that electron transfers of bacterial denitrifiers are more burdensome and more easily disrupted than those in fungal denitrifiers. On the other hand, disturbance to proton H^+ balance in denitrifiers may also be responsible for the different responses between bacteria and fungi. Acidification increases periplasmic H^+ contents in bacterial denitrifiers and disrupts H^+ balance between cytoplasm and periplasm, known as "proton motivation" that supports their denitrifying metabolism (Madigan & Martinko, 2006). By contrast, proton motivation between inner and outer mitochondrion of fungal denitrifiers is steadily relative to bacteria (Madigan & Martinko, 2006), and thus, fungal electron transfers are less affected by acidification.

4 | DISCUSSION

Ocean acidification in estuarine regions is becoming a global concern (Breider et al., 2019; Hurd et al., 2018; Kroeker et al., 2013). As summarized in Figure 6, our study indicates that ocean acidification disturbs microorganism-mediated N cycling and increases N_2O flux from the estuarine region. Furthermore, based on our incubation results, it is suggested that denitrification-derived N_2O emissions would be stimulated by future ocean acidification. Because N_2O can generate a 298-fold effect on global warming compared to CO_2 (IPCC, 2013), the increased N_2O emissions by acidification could potentially influence global climate change in estuaries. We further assessed N_2O emission-based Global Warming Potential (GWP_{N_2O}; Table S8) to evaluate the potential warming effect of N_2O emission from the estuarine ecosystem (Chen et al., 2021; Guo et al., 2020). The GWP_{N_2O} at pH 6.8 (in situ estuarine environment) was 0.68 g CO_2 eq m^{-2} day^{-1}, similar to those of soil ecosystems (0.05–0.72 g CO_2 eq m^{-2} day^{-1}; Chen et al., 2021) but slightly higher than wetland sediments (0.30–0.60 g CO_2 eq m^{-2} day^{-1}; Du et al., 2018). However, the GWP_{N_2O} greatly increased to 2.15 g CO_2 eq m^{-2} day^{-1} at pH 5.8, implying that acidification increases the estuarine warming potential. Thus, our results indicate that actions to reduce anthropogenic-derived pollutants such as CO_2 and N should be taken in the following decades. Otherwise, acidification could negatively affect biogeochemical cycling (e.g., C and N cycling), estuarine ecosystems, and human activities (Breider et al., 2019). It should be noted that although the estimation results of our mechanistic study

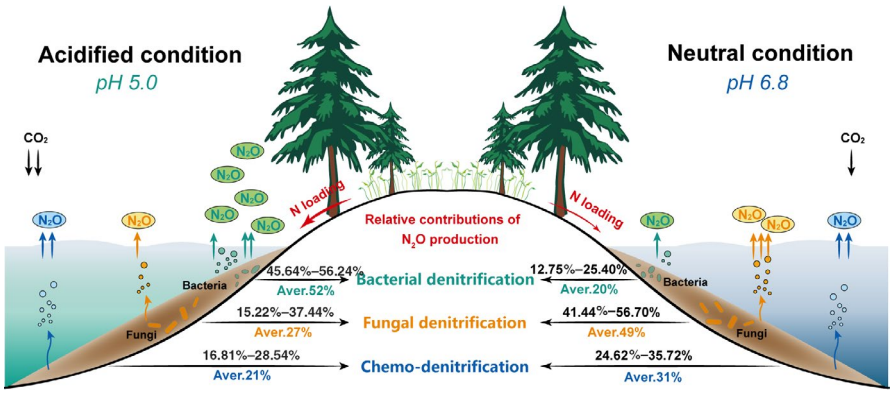

FIGURE 6 Conceptual model of acidification impacts on denitrification-based N_2O production in the estuarine sediment

indicated an increasing N_2O yield by acidification, large-scale field studies are warranted in order to extrapolate N_2O fluxes in global estuarine ecosystems.

Based on the SP of N_2O, acidification changed the production pathways of N_2O (Figures 2 and 6). Our mass balance of N_2O isotope highlighted that fungal denitrification was dominant under neutral conditions and the chemo-denitrification contribution cannot be overlooked in estuarine ecosystems. Thus, we suggest that fungal and chemical N_2O sources may represent significant components when assessing N_2O dynamics in aquatic ecosystems, particularly in regions with N-enriched pollution. Under acidified conditions, however, the major N_2O production pathway shifted to a bacterial source. These results provide a better insight into field assessments of N_2O flux under ocean acidification in estuarine ecosystems. The commonly observed dynamics of N_2O may be comprised of a complex network of diverse contributions by biotic and abiotic pathways (Wankel et al., 2017). Our findings reiterate that these previously under-appreciated sources of N_2O yields should be highlighted when assessing the impacts of acidification on the biogeochemical cycling of N in the future.

ACKNOWLEDGMENTS

We thank Professor James Prosser for the helpful comments on the manuscript. This project was funded by the Science Fund for Creative Research Groups of the National Natural Science Foundation of China (42021005), Natural Science Foundation of China (42003060), the Strategic Priority Research Program of Chinese Academy of Sciences (Y9IXD21A10), and the China Postdoctoral Science Foundation (2019M662253).

CONFLICT OF INTEREST

The authors declare no conflict of interest.

DATA AVAILABILITY STATEMENT

Data are available from the corresponding author upon request.

ORCID

Xiaoxuan Su https://orcid.org/0000-0001-6965-7084
Yong-guan Zhu https://orcid.org/0000-0003-3861-8482

REFERENCES

Baggs, E. M. (2008). A review of stable isotope techniques for N_2O source partitioning in soils: Recent progress, remaining challenges and future considerations. *Rapid Communications in Mass Spectrometry*, *22*, 1664–1672. https://doi.org/10.1002/rcm.3456

Banerjee, S., Schlaeppi, K., & van der Heijden, M. G. A. (2018). Keystone taxa as drivers of microbiome structure and functioning. *Nature Reviews Microbiology*, *16*, 567–576. https://doi.org/10.1038/s41579-018-0024-1

Bedmar, E. J., Robles, E. F., & Delgado, M. J. (2005). The complete denitrification pathway of the symbiotic, nitrogen-fixing bacterium *Bradyrhizobium japonicum*. *Biochemical Society Transactions*, *33*, 141–144. https://doi.org/10.1042/bst0330141

Breider, F., Yoshikawa, C., Makabe, A., Toyoda, S., Wakita, M., Matsui, Y., Kawagucci, S., Fujiki, T., Harada, N., & Yoshida, N. (2019). Response of N_2O production rate to ocean acidification in the western North Pacific. *Nature Climate Change*, *9*, 954–958. https://doi.org/10.1038/s41558-019-0605-7

Broberg, A. (1985). A modified method for studies of electron transport system activity in freshwater sediments. *Hydrobiologia*, *120*, 181–187. https://doi.org/10.1007/bf00032140

Caporaso, J. G., Kuczynski, J., Stombaugh, J., Bittinger, K., Bushman, F. D., Costello, E. K., Fierer, N., Pena, A. G., Goodrich, J. K., Gordon, J. I., Huttley, G. A., Kelley, S. T., Knights, D., Koenig, J. E., Ley, R. E., Lozupone, C. A., McDonald, D., Muegge, B. D., Pirrung, M., … Knight, R. (2010). QIIME allows analysis of high-throughput community sequencing data. *Nature Methods*, *7*, 335–336. https://doi.org/10.1038/nmeth.f.303

Chen, D., Yuan, X., Zhao, W., Luo, X., Li, F., & Liu, T. (2020). Chemodenitrification by Fe (II) and nitrite: pH effect, mineralization and kinetic modeling. *Chemical Geology*, *541*. https://doi.org/10.1016/j.chemgeo.2020.119586

Chen, D., Zhou, Y., Xu, C., Lu, X., Liu, Y., Yu, S., & Feng, Y. (2021). Water-washed hydrochar in rice paddy soil reduces N_2O and CH_4 emissions: A whole growth period investigation. *Environmental Pollution*, *274*, 116573. https://doi.org/10.1016/j.envpol.2021.116573

Chen, Q.-L., Ding, J., Zhu, D., Hu, H.-W., Delgado-Baquerizo, M., Ma, Y.-B., He, J.-Z., & Zhu, Y.-G. (2020). Rare microbial taxa as the major drivers of ecosystem multifunctionality in long-term fertilized soils. *Soil Biology and Biochemistry*, *141*. https://doi.org/10.1016/j.soilbio.2019.107686

Cheung, Y. Y., Cheung, S., Mak, J., Liu, K., Xia, X., Zhang, X., Yung, Y., & Liu, H. (2021). Distinct interaction effects of warming and anthropogenic input on diatoms and dinoflagellates in an urbanized estuarine ecosystem. *Global Change Biology*, *27*, 3463–3473. https://doi.org/10.1111/gcb.15667

Decock, C., & Six, J. (2013). How reliable is the intramolecular distribution of N^{15} in N_2O to source partition N_2O emitted from soil? *Soil Biology and Biochemistry*, *65*, 114–127. https://doi.org/10.1016/j.soilbio.2013.05.012

Douglas, G. M., Maffei, V. J., Zaneveld, J. R., Yurgel, S. N., Brown, J. R., Taylor, C. M., Huttenhower, C., & Langille, M. G. I. (2020). PICRUSt2 for prediction of metagenome functions. *Nature Biotechnology*, *38*, 685–688. https://doi.org/10.1038/s41587-020-0548-6

Du, Y., Pan, K., Yu, C., Luo, B., Gu, W., Sun, H., Min, Y., Liu, D., Geng, Y., Han, W., Chang, S. X., Liu, Y., Li, D., Ge, Y., & Chang, J. (2018). Plant diversity decreases net global warming potential integrating multiple functions in microcosms of constructed wetlands. *Journal of Cleaner Production*, *184*, 718–726. https://doi.org/10.1016/j.jclepro.2018.02.273

Duan, H. R., Ye, L., Erler, D., Ni, B. J., & Yuan, Z. G. (2017). Quantifying nitrous oxide production pathways in wastewater treatment systems using isotope technology—A critical review. *Water Research*, *122*, 96–113. https://doi.org/10.1016/j.watres.2017.05.054

Elshahed, M. S., Youssef, N. H., Spain, A. M., Sheik, C., Najar, F. Z., Sukharnikov, L. O., Roe, B. A., Davis, J. P., Schloss, P. D., Bailey, V. L., & Krumholz, L. R. (2008). Novelty and uniqueness patterns of rare members of the soil biosphere. *Applied and Environmental Microbiology*, *74*, 5422–5428. https://doi.org/10.1128/aem.00410-08

Feely, R. A., Sabine, C. L., Hernandez-Ayon, J. M., Ianson, D., & Hales, B. (2008). Evidence for upwelling of corrosive "acidified" water onto the continental shelf. *Science*, *320*, 1490–1492. https://doi.org/10.1126/science.1155676

Frame, C. H., & Casciotti, K. L. (2010). Biogeochemical controls and isotopic signatures of nitrous oxide production by a marine ammonia-oxidizing bacterium. *Biogeosciences*, *7*, 2695–2709. https://doi.org/10.5194/bg-7-2695-2010

Fry, B. (2006). *Stable isotope ecology*. Springer Science & Business Media.

Galand, P. E., Casamayor, E. O., Kirchman, D. L., & Lovejoy, C. (2009). Ecology of the rare microbial biosphere of the Arctic Ocean.

Proceedings of the National Academy of Sciences of the United States of America, *106*, 22427–22432. https://doi.org/10.1073/pnas.0908284106

Gao, D. Z., Hou, L. J., Liu, M., Li, X. F., Zheng, Y. L., Yin, G. Y., Wu, D. M., Yang, Y., Han, P., Liang, X., & Dong, H. P. (2020). Mechanisms responsible for N_2O emissions from intertidal soils of the Yangtze Estuary. *Science of the Total Environment*, *716*. https://doi.org/10.1016/j.scitotenv.2020.137073

Grossart, H. P., Van den Wyngaert, S., Kagami, M., Wurzbacher, C., Cunliffe, M., & Rojas-Jimenz, K. (2019). Fungi in aquatic ecosystems. *Nature Reviews Microbiology*, *17*, 339–354. https://doi.org/10.1038/s41579-019-0175-8

Guo, F., Zhang, J., Yang, X., He, Q., Ao, L., & Chen, Y. (2020). Impact of biochar on greenhouse gas emissions from constructed wetlands under various influent chemical oxygen demand to nitrogen ratios. *Bioresource Technology*, *303*. https://doi.org/10.1016/j.biortech.2020.122908

Heil, J., Wolf, B., Brüggemann, N., Emmenegger, L., Tuzson, B., Vereecken, H., & Mohn, J. (2014). Site-specific ^{15}N isotopic signatures of abiotically produced N_2O. *Geochimica et Cosmochimica Acta*, *139*, 72–82. https://doi.org/10.1016/j.gca.2014.04.037

Hu, H. W., Chen, D., & He, J. Z. (2015). Microbial regulation of terrestrial nitrous oxide formation: Understanding the biological pathways for prediction of emission rates. *FEMS Microbiology Ecology*, *39*, 729–749. https://doi.org/10.1093/femsre/fuv021

Humbert, G., Sebilo, M., Fiat, J., Lang, L. Q., Filali, A., Vaury, V., Sperandio, M., & Laverman, A. M. (2020). Isotopic evidence for alteration of nitrous oxide emissions and producing pathways' contribution under nitrifying conditions. *Biogeosciences*, *17*, 979–993. https://doi.org/10.5194/bg-17-979-2020

Hurd, C. L., Lenton, A., Tilbrook, B., & Boyd, P. W. (2018). Current understanding and challenges for oceans in a higher-CO_2 world. *Nature Climate Change*, *8*, 686–694. https://doi.org/10.1038/s41558-018-0211-0

IPCC. (2013). *Climate change 2013: The physical science basis* (p. 153). Cambridge University Press.

Joint, I., Doney, S. C., & Karl, D. M. (2011). Will ocean acidification affect marine microbes? *The ISME Journal*, *5*, 1–7. https://doi.org/10.1038/ismej.2010.79

Jones, L. C., Peters, B., Pacheco, J. S. L., Casciotti, K. L., & Fendorf, S. (2015). Stable isotopes and iron oxide mineral products as markers of chemodenitrification. *Environmental Science & Technolology*, *49*, 3444–3452. https://doi.org/10.1021/es504862x

Jung, M.-Y., Gwak, J.-H., Rohe, L., Giesemann, A., Kim, J.-G., Well, R., Madsen, E. L., Herbold, C. W., Wagner, M., & Rhee, S.-K. (2019). Indications for enzymatic denitrification to N_2O at low pH in an ammonia-oxidizing archaeon. *The ISME Journal*, *13*, 2633–2638. https://doi.org/10.1038/s41396-019-0460-6

Kobayashi, M., Matsuo, Y., Takimoto, A., Suzuki, S., Maruo, F., & Shoun, H. (1996). Denitrification, a novel type of respiratory metabolism in fungal mitochondrion. *Journal of Biological Chemistry*, *271*, 16263–16267. https://doi.org/10.1074/jbc.271.27.16263

Koch, M., Bowes, G., Ross, C., & Zhang, X. H. (2013). Climate change and ocean acidification effects on seagrasses and marine macroalgae. *Global Change Biology*, *19*, 103–132. https://doi.org/10.1111/j.1365-2486.2012.02791.x

Kroeker, K. J., Kordas, R. L., Crim, R., Hendriks, I. E., Ramajo, L., Singh, G. S., Duarte, C. M., & Gattuso, J. P. (2013). Impacts of ocean acidification on marine organisms: Quantifying sensitivities and interaction with warming. *Global Change Biology*, *19*, 1884–1896. https://doi.org/10.1111/gcb.12179

Langille, M. G. I., Zaneveld, J., Caporaso, J. G., McDonald, D., Knights, D., Reyes, J. A., Clemente, J. C., Burkepile, D. E., Thurber, R. L. V., Knight, R., Beiko, R. G., & Huttenhower, C. (2013). Predictive functional profiling of microbial communities using 16S rRNA marker gene sequences. *Nature Biotechnology*, *31*, 814–821. https://doi.org/10.1038/nbt.2676

Laughlin, R. J., & Stevens, R. J. (2002). Evidence for fungal dominance of denitrification and codenitrification in a grassland soil. *Soil Science Society of America Journal*, *66*, 1540–1548. https://doi.org/10.2136/sssaj2002.1540

Lee, Y. H., Kang, H.-M., Kim, M.-S., Wang, M., Kim, J. H., Jeong, C.-B., & Lee, J.-S. (2019). Effects of ocean acidification on life parameters and antioxidant system in the marine copepod *Tigriopus japonicus*. *Aquatic Toxicology*, *212*, 186–193. https://doi.org/10.1016/j.aquatox.2019.05.007

Lewicka-Szczebak, D., Augustin, J., Giesemann, A., & Well, R. (2017). Quantifying N_2O reduction to N_2 based on N_2O isotopocules – Validation with independent methods (helium incubation and ^{15}N gas flux method). *Biogeosciences*, *14*, 711–732. https://doi.org/10.5194/bg-14-711-2017

Li, M., Su, Y. L., Chen, Y. G., Wan, R., Zheng, X., & Liu, K. (2016). The effects of fulvic acid on microbial denitrification: Promotion of NADH generation, electron transfer, and consumption. *Applied Microbiology and Biotechnology*, *100*, 5607–5618. https://doi.org/10.1007/s00253-016-7383-1

Liu, B., Morkved, P. T., Frostegard, A., & Bakken, L. R. (2010). Denitrification gene pools, transcription and kinetics of NO, N_2O and N_2 production as affected by soil pH. *FEMS Microbiology Ecology*, *72*, 407–417. https://doi.org/10.1111/j.1574-6941.2010.00856.x

Lynch, M. D. J., & Neufeld, J. D. (2015). Ecology and exploration of the rare biosphere. *Nature Reviews Microbiology*, *13*, 217–229. https://doi.org/10.1038/nrmicro3400

Madigan, M. T., & Martinko, J. M. (2006). *Brock biology of microorganisms*. Pearson Education.

Maeda, K., Spor, A., Edel-Hermann, V., Heraud, C., Breuil, M.-C., Bizouard, F., Toyoda, S., Yoshida, N., Steinberg, C., & Philippot, L. (2015). N_2O production, a widespread trait in fungi. *Scientific Reports*, *5*. https://doi.org/10.1038/srep09697

Maeda, K., Toyoda, S., Philippot, L., Hattori, S., Nakajima, K., Ito, Y., & Yoshida, N. (2017). Relative contribution of nirK- and nirS-bacterial denitrifiers as well as fungal denitrifiers to nitrous oxide production from dairy manure compost. *Environmental Science & Technology*, *51*, 14083–14091. https://doi.org/10.1021/acs.est.7b04017

McTigue, N. D., Gardner, W. S., Dunton, K. H., & Hardison, A. K. (2016). Biotic and abiotic controls on co-occurring nitrogen cycling processes in shallow Arctic shelf sediments. *Nature Communications*, *7*, 1–11. https://doi.org/10.1038/ncomms13145

Mothapo, N., Chen, H., Cubeta, M. A., Grossman, J. M., Fuller, F., & Shi, W. (2015). Phylogenetic, taxonomic and functional diversity of fungal denitrifiers and associated N_2O production efficacy. *Soil Biology and Biochemistry*, *83*, 160–175. https://doi.org/10.1016/j.soilbio.2015.02.001

Nagashima, S., Kamimura, A., Shimizu, T., Nakamura-Isaki, S., Aono, E., Sakamoto, K., Ichikawa, N., Nakazawa, H., Sekine, M., Yamazaki, S., Fujita, N., Shimada, K., Hanada, S., & Nagashima, K. V. P. (2012). Complete genome sequence of phototrophic Betaproteobacterium Rubrivivax gelatinosus IL144. *Journal of Bacteriology*, *194*, 3541–3542. https://doi.org/10.1128/jb.00511-12

Ostrom, N. E., Pitt, A., Sutka, R., Ostrom, P. H., Grandy, A. S., Huizinga, K. M., & Robertson, G. P. (2007). Isotopologue effects during N_2O reduction in soils and in pure cultures of denitrifiers. *Journal of Geophysical Research-Biogeosciences*, *112*, 1–12. https://doi.org/10.1029/2006jg000287

Pan, Y., Ye, L., Ni, B.-J., & Yuan, Z. (2012). Effect of pH on N_2O reduction and accumulation during denitrification by methanol utilizing denitrifiers. *Water Research*, *46*, 4832–4840. https://doi.org/10.1016/j.watres.2012.06.003

Pettay, D. T., Gonski, S. F., Cai, W.-J., Sommerfield, C. K., & Ullman, W. J. (2020). The ebb and flow of protons: A novel approach for the

assessment of estuarine and coastal acidification. *Estuarine Coastal and Shelf Science*, *236*. https://doi.org/10.1016/j.ecss.2020.106627

Rees, A. P., Brown, I. J., Jayakumar, A., & Ward, B. B. (2016). The inhibition of N_2O production by ocean acidification in cold temperate and polar waters. *Deep-Sea Research Part II-Topical Studies in Oceanography*, *127*, 93–101. https://doi.org/10.1016/j.dsr2.2015.12.006

Rittmann, B. E., & McCarty, P. L. (2001). *Environmental biotechnology: Principles and applications*. McGraw-Hill.

Rohe, L., Well, R., & Lewicka-Szczebak, D. (2017). Use of oxygen isotopes to differentiate between nitrous oxide produced by fungi or bacteria during denitrification. *Rapid Communications in Mass Spectrometry*, *31*, 1297–1312. https://doi.org/10.1002/rcm.7909

Rousk, J., Baath, E., Brookes, P. C., Lauber, C. L., Lozupone, C., Caporaso, J. G., Knight, R., & Fierer, N. (2010). Soil bacterial and fungal communities across a pH gradient in an arable soil. *The ISME Journal*, *4*, 1340–1351. https://doi.org/10.1038/ismej.2010.58

Samarkin, V. A., Madigan, M. T., Bowles, M. W., Casciotti, K. L., Priscu, J. C., McKay, C. P., & Joye, S. B. (2010). Abiotic nitrous oxide emission from the hypersaline Don Juan Pond in Antarctica. *Nature Geoscience*, *3*, 341–344. https://doi.org/10.1038/ngeo847

Seo, D. C., & DeLaune, R. D. (2010). Fungal and bacterial mediated denitrification in wetlands: Influence of sediment redox condition. *Water Research*, *44*, 2441–2450. https://doi.org/10.1016/j.watres.2010.01.006

Shoun, H., Fushinobu, S., Jiang, L., Kim, S. W., & Wakagi, T. (2012). Fungal denitrification and nitric oxide reductase cytochrome P450nor. *Philosophical Transactions of the Royal Society B-Biological Sciences*, *367*, 1186–1194. https://doi.org/10.1098/rstb.2011.0335

Shoun, H., & Tanimoto, T. (1991). Denitrification by the fungus *Fusarium Oxysporum* and involvement of cytochrome-p450 in the respiratory nitrite reduction. *Journal of Biological Chemistry*, *266*, 11078–11082. https://doi.org/10.1016/S0021-9258(18)99130-1

Su, X., Chen, Y., Wang, Y., Yang, X., & He, Q. (2019a). Impacts of chlorothalonil on denitrification and N_2O emission in riparian sediments: Microbial metabolism mechanism. *Water Research*, *148*, 188–197. https://doi.org/10.1016/j.watres.2018.10.052

Su, X. X., Chen, Y., Wang, Y. Y., Yang, X. Y., & He, Q. (2019b). Disturbances of electron production, transport and utilization caused by chlorothalonil are responsible for the deterioration of soil denitrification. *Soil Biology and Biochemistry*, *134*, 100–107. https://doi.org/10.1016/j.soilbio.2019.03.024

Su, X., Yang, X., Li, H., Wang, H., Wang, Y., Xu, J., Ding, K., & Zhu, Y.-G. (2021). Bacterial communities are more sensitive to ocean acidification than fungal communities in estuarine sediments. *FEMS Microbiology Ecology*, https://doi.org/10.1093/femsec/fiab058

Sun, X., Jayakumar, A., Tracey, J. C., Wallace, E., Kelly, C. L., Casciotti, K. L., & Ward, B. B. (2020). Microbial N_2O consumption in and above marine N_2O production hotspots. *The ISME Journal*, *15*, 1434–1444. https://doi.org/10.1038/s41396-020-00861-2

Sutka, R. L., Adams, G. C., Ostrom, N. E., & Ostrom, P. H. (2008). Isotopologue fractionation during N_2O production by fungal denitrification. *Rapid Communications in Mass Spectrometry*, *22*, 3989–3996. https://doi.org/10.1002/rcm.3820

Sutka, R. L., Ostrom, N. E., Ostrom, P. H., Breznak, J. A., Gandhi, H., Pitt, A. J., & Li, F. (2006). Distinguishing nitrous oxide production from nitrification and denitrification on the basis of isotopomer abundances. *Applied and Environmental Microbiology*, *72*, 638–644. https://doi.org/10.1128/aem.72.1.638-644.2006

Tan, E. H., Zou, W. B., Zheng, Z. Z., Yan, X. L., Du, M. G., Hsu, T. C., Tian, L., Middelburg, J. J., Trull, T. W., & Kao, S. J. (2020). Warming stimulates sediment denitrification at the expense of anaerobic ammonium oxidation. *Nature Climate Change*, *10*, 349–357. https://doi.org/10.1038/s41558-020-0723-2

Tian, H., Xu, R., Canadell, J. G., Thompson, R. L., Winiwarter, W., Suntharalingam, P., Davidson, E. A., Ciais, P., Jackson, R. B., Janssens-Maenhout, G., Prather, M. J., Regnier, P., Pan, N., Pan, S., Peters, G. P., Shi, H., Tubiello, F. N., Zaehle, S., Zhou, F., … Yao, Y. (2020). A comprehensive quantification of global nitrous oxide sources and sinks. *Nature*, *586*, 248. https://doi.org/10.1038/s41586-020-2780-0

Toyoda, S., Mutobe, H., Yamagishi, H., Yoshida, N., & Tanji, Y. (2005). Fractionation of N_2O isotopomers during production by denitrifier. *Soil Biology and Biochemistry*, *37*, 1535–1545. https://doi.org/10.1016/j.soilbio.2005.01.009

Toyoda, S., Yoshida, N., & Koba, K. (2017). Isotopocule analysis of biologically produced nitrous oxide in various environments. *Mass Spectrometry Reviews*, *36*, 135–160. https://doi.org/10.1002/mas.21459

Toyoda, S., Yoshida, N., Miwa, T., Matsui, Y., Yamagishi, H., Tsunogai, U., Nojiri, Y., & Tsurushima, N. (2002). Production mechanism and global budget of N_2O inferred from its isotopomers in the western North Pacific. *Geophysical Research Letters*, *29*. https://doi.org/10.1029/2001gl014311

Uchimura, H., Enjoji, H., Seki, T., Taguchi, A., Takaya, N., & Shoun, H. (2002). Nitrate reductase-formate dehydrogenase couple involved in the fungal denitrification by *Fusarium oxysporum*. *Journal of Biochemistry*, *131*, 579–586. https://doi.org/10.1093/oxfordjournals.jbchem.a003137

Velvis, H. (1997). Evaluation of the selective respiratory inhibition method for measuring the ratio of fungal:bacterial activity in acid agricultural soils. *Biology and Fertility of Soils*, *25*, 354–360. https://doi.org/10.1007/s003740050325

Vial, L., Lavire, C., Mavingui, P., Blaha, D., Haurat, J., Moenne-Loccoz, Y., Bally, R., & Wisniewski-Dye, F. (2006). Phase variation and genomic architecture changes in Azospirillum. *Journal of Bacteriology*, *188*, 5364–5373. https://doi.org/10.1128/jb.00521-06

Waldbusser, G. G., Voigt, E. P., Bergschneider, H., Green, M. A., & Newell, R. I. E. (2011). Biocalcification in the eastern oyster (*Crassostrea virginica*) in relation to long-term trends in Chesapeake bay pH. *Estuaries and Coasts*, *34*, 221–231. https://doi.org/10.1007/s12237-010-9307-0

Wan, R., Chen, Y. G., Zheng, X., Su, Y. L., & Li, M. (2016). Effect of CO_2 on microbial denitrification via inhibiting electron transport and consumption. *Environmental Science & Technology*, *50*, 9915–9922. https://doi.org/10.1021/acs.est.5b05850

Wang, S. Y., Pi, Y. X., Jiang, Y. Y., Pan, H. W., Wang, X. X., Wang, X. M., Zhou, J. M., & Zhu, G. B. (2020). Nitrate reduction in the reed rhizosphere of a riparian zone: From functional genes to activity and contribution. *Environmental Research*, *180*. https://doi.org/10.1016/j.envres.2019.108867

Wang, S. Y., Pi, Y. X., Song, Y. P., Jiang, Y. Y., Zhou, L. G., Liu, W. Y., & Zhu, G. B. (2020). Hotspot of dissimilatory nitrate reduction to ammonium (DNRA) process in freshwater sediments of riparian zones. *Water Research*, *173*. https://doi.org/10.1016/j.watres.2020.115539

Wankel, S. D., Ziebis, W., Buchwald, C., Charoenpong, C., de Beer, D., Dentinger, J., Xu, Z., & Zengler, K. (2017). Evidence for fungal and chemodenitrification based N_2O flux from nitrogen impacted coastal sediments. *Nature Communications*, *8*. https://doi.org/10.1038/ncomms15595

Wannicke, N., Frey, C., Law, C. S., & Voss, M. (2018). The response of the marine nitrogen cycle to ocean acidification. *Global Change Biology*, *24*, 5031–5043. https://doi.org/10.1111/gcb.14424

Watmough, N. J., Field, S. J., Hughes, R. J. L., & Richardson, D. J. (2009). The bacterial respiratory nitric oxide reductase. *Biochemical Society Transactions*, *37*, 392–399. https://doi.org/10.1042/bst0370392

Wei, J., Ibraim, E., Bruggemann, N., Vereecken, H., & Mohn, J. (2019). First real-time isotopic characterisation of N_2O from chemodenitrification. *Geochimica et Cosmochimica Acta*, *267*, 17–32. https://doi.org/10.1016/j.gca.2019.09.018

Wu, D., Fu, M., & Ma, L. (2012). Nitrous oxide emission and control in biological and chemical denitrification. *Progress in Chemistry* (in Chinese), *24*, 2054–2061.

Yu, L., Harris, E., Lewicka-Szczebak, D., Barthel, M., Blomberg, M. R. A., Harris, S. J., Johnson, M. S., Lehmann, M. F., Liisberg, J., Müller, C., Ostrom, N. E., Six, J., Toyoda, S., Yoshida, N., & Mohn, J. (2020). What can we learn from N_2O isotope data? – Analytics, processes and modelling. *Rapid Communications in Mass Spectrometry*, *34*, e8858. https://doi.org/10.1002/rcm.8858

Zheng, B., Zhu, Y., Sardans, J., Penuelas, J., & Su, J. (2018). QMEC: A tool for high-throughput quantitative assessment of microbial functional potential in C, N, P, and S biogeochemical cycling. *Science China-Life Sciences*, *61*, 1451–1462. https://doi.org/10.1007/s11427-018-9364-7

Zhong, Z., Lemke, R. L., & Nelson, L. M. (2009). Nitrous oxide emissions associated with nitrogen fixation by grain legumes. *Soil Biology and Biochemistry*, *41*, 2283–2291. https://doi.org/10.1016/j.soilbio.2009.08.009

Zou, Y., Hirono, Y., Yanai, Y., Hattori, S., Toyoda, S., & Yoshida, N. (2014). Isotopomer analysis of nitrous oxide accumulated in soil cultivated with tea (*Camellia sinensis*) in Shizuoka, central Japan. *Soil Biology and Biochemistry*, *77*, 276–291. https://doi.org/10.1016/j.soilbio.2014.06.016

Zumft, W. G. (1997). Cell biology and molecular basis of denitrification. *Microbiology and Molecular Biology Reviews*, *61*, 533–616. https://doi.org/10.1128/.61.4.533-616.1997

SUPPORTING INFORMATION

Additional supporting information may be found online in the Supporting Information section.

How to cite this article: Su, X., Wen, T., Wang, Y., Xu, J., Cui, L., Zhang, J., Xue, X., Ding, K., Tang, Y., & Zhu, Y.-G. (2021). Stimulation of N_2O emission via bacterial denitrification driven by acidification in estuarine sediments. *Global Change Biology*, 00, 1–16. https://doi.org/10.1111/gcb.15863